atmosphere

MDPI

Article

Characteristics and Weekend Effect of Air Pollution in Eastern Jilin Province

Chunsheng Fang, Kexin Xue, Juan Li and Ju Wang *

College of New Energy and Environment, Jilin University, Changchun 130012, China; fangcs@jlu.edu.cn (C.F.); xuekx20@mails.jlu.edu.cn (K.X.); lijuan21@mails.jlu.edu.cn (J.L.)
* Correspondence: wangju@jlu.edu.cn; Tel.: +86-0-13104317228

Abstract: Using the hourly monitoring data of pollutants from 16 automatic atmospheric monitoring stations in eastern Jilin Province from 2015 to 2020, this paper analyzed the temporal and spatial distribution laws of CO, SO_2, NO_2, PM_{10}, $PM_{2.5}$, and O_3 in eastern Jilin Province. At the same time, the regional transport pathways of pollutants were analyzed using the hybrid single-particle Lagrangian integrated trajectory (HYSPLIT) model; the potential source contribution function (PSCF) analyzed the potential source area of $PM_{2.5}$. Finally, the "weekend effect" of CO, NO_2, $PM_{2.5}$, and O_3 was analyzed. The results showed that the six pollutants showed a downward trend year by year. The concentrations of O_3, PM_{10}, and $PM_{2.5}$ were higher in northwest Jilin, and the concentrations of SO_2 and CO were higher in southwest Jilin. Except for CO, the seasonal variation of pollutants was pronounced. Except for O_3, most pollutants had the highest concentration in winter. Hourly variation analysis described that SO_2 and O_3 had only one peak in a day, and the other four pollutants showed "double peak" hourly variation characteristics. The study area was mainly affected by the airflow pathway from northwest and southwest. The weight potential source contribution function (WPSCF) high-value area of $PM_{2.5}$ was northwest and southwest. O_3 showed a "negative weekend effect", and NO_2 and CO showed a "positive weekend effect".

Keywords: temporal and spatial distribution; air pollution; backward trajectory; weekend effect

Citation: Fang, C.; Xue, K.; Li, J.; Wang, J. Characteristics and Weekend Effect of Air Pollution in Eastern Jilin Province. *Atmosphere* **2022**, *13*, 681. https://doi.org/10.3390/atmos13050681

Academic Editor: Ilias Kavouras

Received: 27 March 2022
Accepted: 21 April 2022
Published: 24 April 2022

1. Introduction

The air pollution problem worsens the quality of the atmospheric environment and harms people's lives, work, health, and ecological environment [1]. $PM_{2.5}$ is particulate matter with a particle diameter less than or equal to 2.5 μm. Its complex chemical composition can cause many diseases, such as cardiovascular and cerebrovascular diseases and respiratory diseases [2]. SO_2 and NO_2 are precursors for the formation of particles and cause the acidification of the atmosphere and soil. They also produce secondary pollutants such as O_3 [3]. O_3 can accelerate the construction of pollutants such as particulate matter and affect the frequency and intensity of heavily polluted weather [4]. At the same time, it will have adverse effects on the ecosystem, human health [5], and crops [6,7] within a specific concentration range. Therefore, it is crucial to solve the problem of air pollution, which has become one of the hotspots of scholars' research.

With the development of the economy, urbanization is gradually accelerated, but urbanization may increase the degree of environmental pollution. For example, the environmental pollution in China's big cities is the most serious [8]. In northern China, coal-fired heating in winter leads to a significant increase in pollutant emissions. At the same time, the relatively stable weather conditions in winter make it impossible for pollutants to be diluted quickly, resulting in a further increase in the degree of air pollution in autumn and winter.

At present, China's air quality is not positive. The Chinese government has implemented stricter policies and regulations to control air pollution [9]. See Table 1 for the

annual average class II concentration limit of pollutants in China's Ambient Air Quality Standard (GB3905-2012). The five-year emission reduction targets of $PM_{2.5}$ from 2013 to 2017 were set in China's most economically developed regions, including the Beijing Tianjin Hebei region in northern China, the Yangtze River Delta in eastern China, and the Pearl River Delta in southern China. Except for $PM_{2.5}$, common air pollutants include CO, SO_2, NO_2, PM_{10}, and O_3.

Table 1. The concentration limit in China's "Ambient Air Quality Standards" (GB3905-2012).

City	NO_2	SO_2	$PM_{2.5}$	PM_{10}
Annual average secondary concentration limit ($\mu g/m^3$)	40	60	35	70
Annual average primary concentration limit ($\mu g/m^3$)	40	20	15	40
Level I 24 h concentration standard ($\mu g/m^3$)	80	50	35	50
Secondary 24 h concentration standard ($\mu g/m^3$)	80	150	75	150

It is necessary to use accurate air pollutant monitoring devices to know the actual air quality. Different sensors will lead to different data quality [10], especially $PM_{2.5}$. Our study used the automatic monitoring data of six conventional pollutants from 2015 to 2020, 48i, 49iQ, 43iQ, 42iQ, and 5030i, of Thermo Scientific equipment to monitor CO, O_3, SO_2, NO_2, and $PM_{2.5}/PM_{10}$, respectively. The monitor used the infrared absorption method to measure CO; O_3 in ambient air was measured using double-cell UV spectrophotometry. The measurement of SO_2 was carried out using the pulsed fluorescence technique; NO_2 was measured using chemiluminescence technology; the monitor adopted a non-stop measurement method, combining the light scattering turbidity method and the β Ray absorption method, which measured $PM_{2.5}$ and PM_{10}. The measurement range of the 5030i monitor is 0–10,000 $\mu g/m^3$. When the concentration is less than 80 $\mu g/m^3$, the accuracy is ± 2.0 $\mu g/m^3$. When the concentration is more than 80 $\mu g/m^3$, the accuracy is ± 5 $\mu g/m^3$, and the mass measurement error is within ±5%.At present, research on the characteristics of air pollution is mainly concentrated in areas with rapid economic development, such as Beijing Tianjin Hebei [11–13], Yangtze River Delta [14,15], and Pearl River Delta [16], and there is less research on the eastern part of Jilin Province. In this context, using the automatic monitoring data of six conventional pollutants from 2015 to 2020, this paper analyzed the temporal and spatial distribution law of air pollutants in the eastern part of Jilin Province and found potential pollution source areas. At the same time, to understand whether the air pollution in this area is related to human activities, this paper analyzed the characteristics of the "weekend effect." The above research provided theoretical support for the formulation of reasonable air pollution control measures in the eastern part of Jilin Province.

2. Materials and Methods

2.1. Study Area and Data Source

The eastern part of Jilin Province includes Jilin City, Liaoyuan City, Tonghua City, Baishan City, and Yanbian Korean Autonomous Prefecture, with about 108,668 square kilometers and a permanent population of about 11.37 million. See Tables S1 and S2 for detailed information and the main economic activities in the eastern part of Jilin Province. The eastern part of Jilin Province belongs to a temperate, semi-humid, continental climate, with significant temperature differences throughout the year and four distinct seasons. The eastern part of Jilin Province had the highest temperature in July, with an average temperature of 17.78 °C, an average maximum temperature of 21.02 °C, and an average minimum temperature of 21.94 °C. The temperature in January was the lowest of the whole year, and the average temperature reached −15.16 °C. The precipitation in July was the highest, reaching 182.48 mm, followed by June and August. The monthly average relative humidity in the study area showed a single peak and double valley type, with the maximum from July to August and the lowest from March to April and October to November.

This study used the mass concentrations of six conventional pollutants ($PM_{2.5}$, PM_{10}, CO, SO_2, NO_2, and O_3) from 2 January 2015 to 31 December 2020, from 16 air quality monitoring stations in the eastern part of Jilin Province (Figure 1). The specific information of 16 air quality monitoring stations is shown in Table 2. The particular locations of the 16 monitoring stations are shown in Figure 2. 48i, 49iQ, 43iQ, 42iQ, and 5030i of Thermo Scientific equipment were used to monitor CO, O_3, SO_2, NO_2, and $PM_{2.5}$/PM_{10}, respectively. Hourly monitoring data were used for the analysis of six pollutants. In this paper, all data were preprocessed according to the "Monitoring Regulation for Ambient Air Quality" (HJ/T193-2005) to eliminate spatial and temporal outliers and ensure data quality [17]. Spring was defined as March, April, and May. Summer was defined as June, July, and August. Autumn was defined as September, October, and November. Winter was defined as December, January, and February. According to the notice on holiday arrangement issued by the general office of the State Council, the 16–19 years were divided into working days and holidays for "weekend effect" analysis.

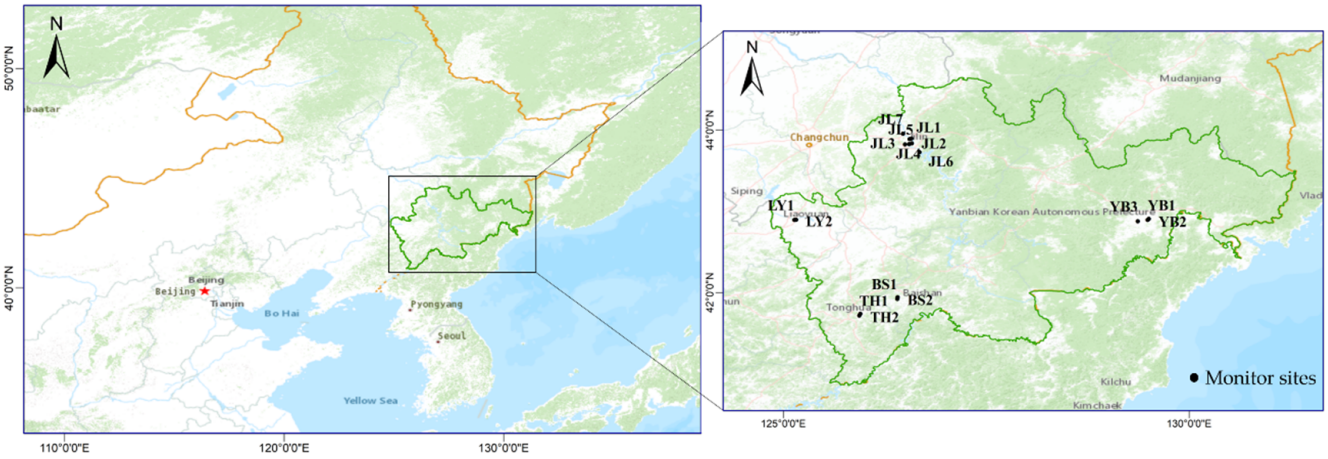

Figure 1. Air quality inspection station in eastern Jilin Province.

Table 2. Specific information regarding monitoring stations.

Monitoring Station	City	East Longitude	North Latitude	Location
LY1	Liaoyuan	125.1358	42.8947	Environmental Protection Bureau
LY2	Liaoyuan	125.1567	42.8953	Sewage Treatment Plant
TH1	Tonghua	125.9361	41.7156	River
TH2	Tonghua	125.9486	41.7381	Dongchang District
BS1	Baishan	126.4047	41.9206	Industrial zone
BS2	Baishan	126.4078	41.9419	Residence community
YB1	Yanbian	129.4892	42.8939	Hospital
YB2	Yanbian	129.5042	42.9061	Yanbian Hospital
YB3	Yanbian	129.3675	42.8775	Chaoyang Chuanzhen Hospital
JL1	Jilin	126.555	43.8875	Downtown area
JL2	Jilin	126.5844	43.8358	Beihua University
JL3	Jilin	126.4978	43.8228	Electric Power College
JL4	Jilin	126.5786	43.8947	Second Songhua Jiang
JL5	Jilin	126.55	43.8256	Jiangnan Park
JL6	Jilin	126.6772	43.7256	Tourist area
JL7	Jilin	126.6772	43.7256	Industrial zone

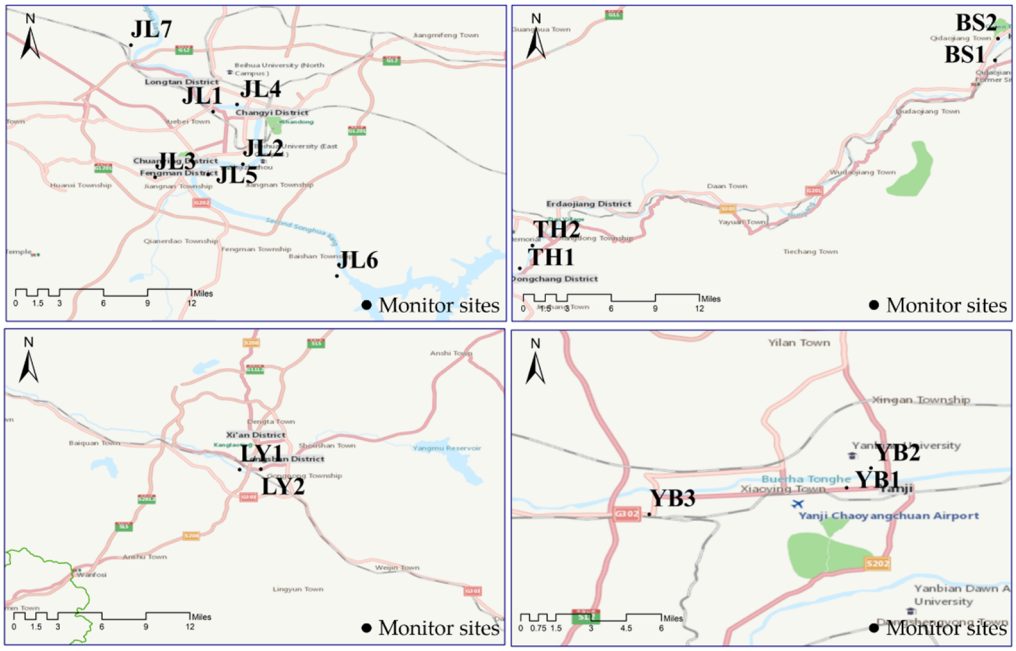

Figure 2. The specific location of monitoring stations in the east of Jilin Province.

2.2. Analysis of Temporal and Spatial Distribution Characteristics

Based on the pollutant concentrations observed at 16 monitoring stations, the Kriging interpolation method in Surfer software (Golden Software, Golden, CO, USA) was used to draw the contour map of six kinds of pollutant concentrations in the study area over 6 years. Because the distribution of sampling points is discrete and the sample data obtained is limited, it cannot show the distribution state of pollutants in the whole region, and the Kriging interpolation algorithm can adequately solve the assignment problem from point to surface. Kriging interpolation uses the distance and spatial direction between known sample points to reflect the spatial correlation and makes a linear unbiased optimal prediction for the unknown points [18]. However, Kriging interpolation is an inverse distance interpolation method, so the distance and density between monitoring points will affect the model's accuracy. For example, the distance between some monitoring points in this study was far, which increased the gap between the simulated value and the actual value to a certain extent. The spatial changes in six pollutants were analyzed according to the image. At the same time, the annual average concentrations of six pollutants in six years were calculated, and we explored the difference in pollutant concentration between years.

The inter-group connection method in SPSS (statistical product and service solutions) software system clustering was used to cluster each site. There are slight differences in each component in the same cluster and significant differences in different collections. The SPSS software package implements the Ward1 algorithm [19]. The square Euclidean distance was selected for clustering to generate a correct tree view to verify the spatial distribution difference of pollutants. This paper divided a year into four seasons: spring, summer, autumn, and winter, and analyzed the hourly variation of different pollutants in different seasons. Further, we divided the stations according to cities and explored the hourly variation trend of contaminants in each city. Finally, the average concentrations of six pollutants each month were superimposed to analyze the monthly changes.

2.3. Backward Trajectory and Potential Source Area Analysis

To generate 72 h backward air mass trajectories approaching the eastern region of Jilin Province at 500 m high above ground level (AGL) over the whole year of 2019, the HYSPLIT model was applied [20]. The meteorological data used in the backward trajectory model were the simultaneous global data assimilation system (GDAS) data ($1° \times 1°$) provided by the National Center for environmental prediction (NCEP). The trajectories' arrival

point was the JL1 monitoring station (126.555° E, 43.8875° N). Additionally, the transport and dilution trajectories of air pollutants were analyzed. This study used the stepwise cluster analysis method [21] to classify and summarize the trajectories to obtain the average trajectories that can represent multiple trajectories. In this paper, the optimal number of clusters was determined by observing the spatial change rate. The larger the spatial change rate, the more significant the difference between the current trajectory clusters. In other words, the number of clusters is more reasonable.

To identify the potential source areas of PM $_{2.5}$ and provide theoretical support for the regional joint treatment of air pollutants in the eastern part of Jilin Province, we implemented the potential source contribution function (PSCF) for PM $_{2.5}$ in this study. PSCF was calculated based on the concentration data of $PM_{2.5}$ in 2019 [22]. $PM_{2.5}$ limit concentration was taken from the secondary standard limit in *ambient air quality standard (GB3905-2012)*, which is 75 $\mu g/m^3$. PSCF is represented by Equation (1):

$$PSCF_{ij} = \frac{m_{ij}}{n_{ij}} \tag{1}$$

In Equation (1), n_{ij} is the sum of the transportation time of all trajectories when passing through the grid (i, j), and m_{ij} is the sum of the transportation time of trajectories whose concentration exceeds the limit of the grid (i, j). The value of PSCF reflects the possibility that the air pollutant concentration exceeds the standard value when the air mass passes through the grid. Because PSCF is a conditional probability function, the calculated PSCF value will have great uncertainty for some meshes with few trajectories. In order to reduce the error and make the result more accurate, the weighting function W_{ij} was introduced to obtain WPSCF [23]. In this study, W_{ij} is represented by Equation (2):

$$W_{ij} = \begin{cases} 1.0 & n_{ij} > 90 \\ 0.7 & 45 < n_{ij} \leq 90 \\ 0.4 & 30 < n_{ij} \leq 45 \\ 0.2 & n_{ij} \leq 30 \end{cases} \tag{2}$$

At the same time, the potential source area of $PM_{2.5}$ was verified again using concentration-weighted trajectory (CWT) [24]. The difference between CWT and PSCF is that PSCF uses a concentration threshold to evaluate the potential source of $PM_{2.5}$. This means that when the sample concentration is only slightly higher or much higher than the standard, its PSCF value may be the same. Therefore, it may not be able to distinguish between medium and potent sources. For the CWT method, the weighted concentration can be allocated by averaging the sample concentration with the relevant trajectory passing through the grid cell to overcome the limitation of PSCF. CWT is represented by Equation (3):

$$C_{ij} = \frac{\sum_{l=1}^{M} C_l \tau_{ijl}}{\sum_{l=1}^{M} \tau_{ijl}} \tag{3}$$

In Equation (3), C_{ij} is the average weight concentration in the grid (i, j), l is the trajectory index, C_l is the pollutant concentration measured when track l arrives, and M is the total number of trajectories. τ_{ijl} is the time that the trajectory l stays in the grid (i, j). The higher the C_{ij} value, the more significant the trajectory's contribution to the study area's air pollution.

2.4. Weekend Effect Analysis

There are many ways to define the "weekend effect." Some studies have defined the weekend effect as the average value from Saturday to Monday minus the average from Wednesday to Friday or directly compared the weekend concentration with the working

day concentration [25,26]. WE was adopted in this paper to quantify the weekend effect. WE is represented by Equation (4):

$$WE = \left[\frac{C_{weekend} - C_{working\ day}}{C_{working\ day}} \right] \times 100\% \quad (4)$$

In the formula, $C_{weekend}$ and $C_{working\ day}$ represent the weekend hourly mean concentration and working day hourly mean concentration of pollutants. This method has been adopted by many studies [27,28]. Weekends in this article were legal holidays stipulated by the State Council. In addition, other days were defined as working days. In this study, the average concentrations of CO, NO_2, $PM_{2.5}$, and O_3 on weekends and working days at each station in 16–19 years were calculated, and we calculated the weekend effect. At the same time, the eastern part of Jilin Province was regarded as a whole to analyze the change in the weekend effect between years. If the WE value is positive, it indicates that the pollutant concentration on weekends is greater than that on weekdays, which is defined as a "positive weekend effect". If the WE value is negative, it is defined as a "negative weekend effect", and WE's absolute value represents the intensity of the "weekend effect".

3. Results and Discussions

3.1. Analysis of Temporal and Spatial Distribution Characteristics of Six Air Pollutants

3.1.1. Differences in the Spatial Distribution of Pollutant Concentrations and Annual Changes

Figure 3 analyzes the annual distributions of six pollutant concentrations in the eastern part of Jilin Province from 2015 to 2020. It should be noted that there were few monitoring points in the study area, and most of them were scattered around the area. There were no monitoring points in the center of the study area, resulting in certain uncertainty in the concentration after Kriging interpolation in the center area. The average residuals of the six pollutants at the monitoring points were: CO (0.00007); SO_2 (0.00401); NO_2 (0.00681); $PM_{2.5}$ (0.00242); O_3 (−0.00106); PM_{10} (0.00856) (CO unit: mg/m^3, others are $\mu g/m^3$). The contour map of the annual average O_3 value used the six-year average of the maximum daily value of O_3, and the other five pollutants used the average of all hourly data in six years. Because O_3 has pretty acute solid toxicity, its nature is unstable and it easily decomposes in the atmosphere. At the same time, it is a necessary condition for the formation of photochemical smog. Therefore, the daily maximum O_3 concentration value was used to explore O_3's temporal and spatial distribution. The concentration of O_3 was higher in the northwest region, which might be due to the Songhua Lake National Scenic Spot in the northwest region, facing the water on three sides, surrounded by mountains and good vegetation coverage. The deposition mechanism on the surface of vegetation leaves and the exchange mechanism of soluble air pollutants in stomata during photosynthesis consume some contaminants such as SO_2 and NO_2 and release many O_3 precursors such as volatile organic compounds (VOCs). These biological volatile organic compounds react with nitrogen oxides to increase the O_3 concentration [29].

PM_{10} and $PM_{2.5}$ were seriously polluted in the northwest, which may be related to the relatively developed construction industry in Jilin City. In 2020, the output value of the construction industry in Jilin city reached CNY 9.06 billion, while the output value of the construction industry in the Yanbian area with the most significant size and the lightest particulate pollution was only CNY 5.473 billion. Therefore, it is speculated that the construction industry in Jilin has produced a large amount of dust, resulting in the increase in PM_{10}. In 2020, the power generation of Jilin city reached 13.87 billion kWh, while that of the Yanbian area was only 5.1 billion kWh. The incomplete combustion of coal in the power generation process releases many fine particles, increasing $PM_{2.5}$ concentration. As a result, PM_{10} and $PM_{2.5}$ are higher in the northwest and lower in the southeast. The spatial distribution of PM_{10} and $PM_{2.5}$ was highly consistent, indicating that PM_{10} contains a considerable portion of $PM_{2.5}$ [30].

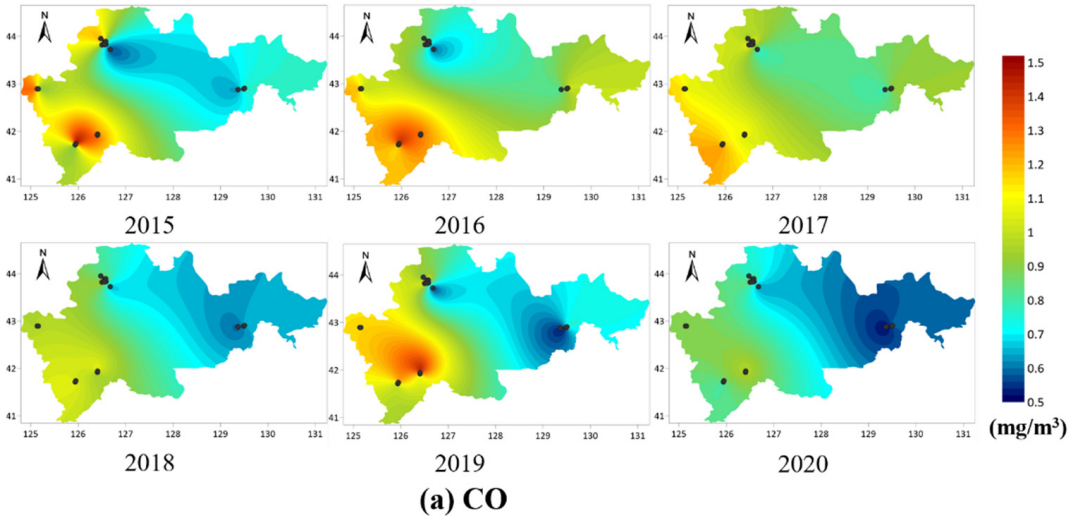

Figure 3. *Cont*.

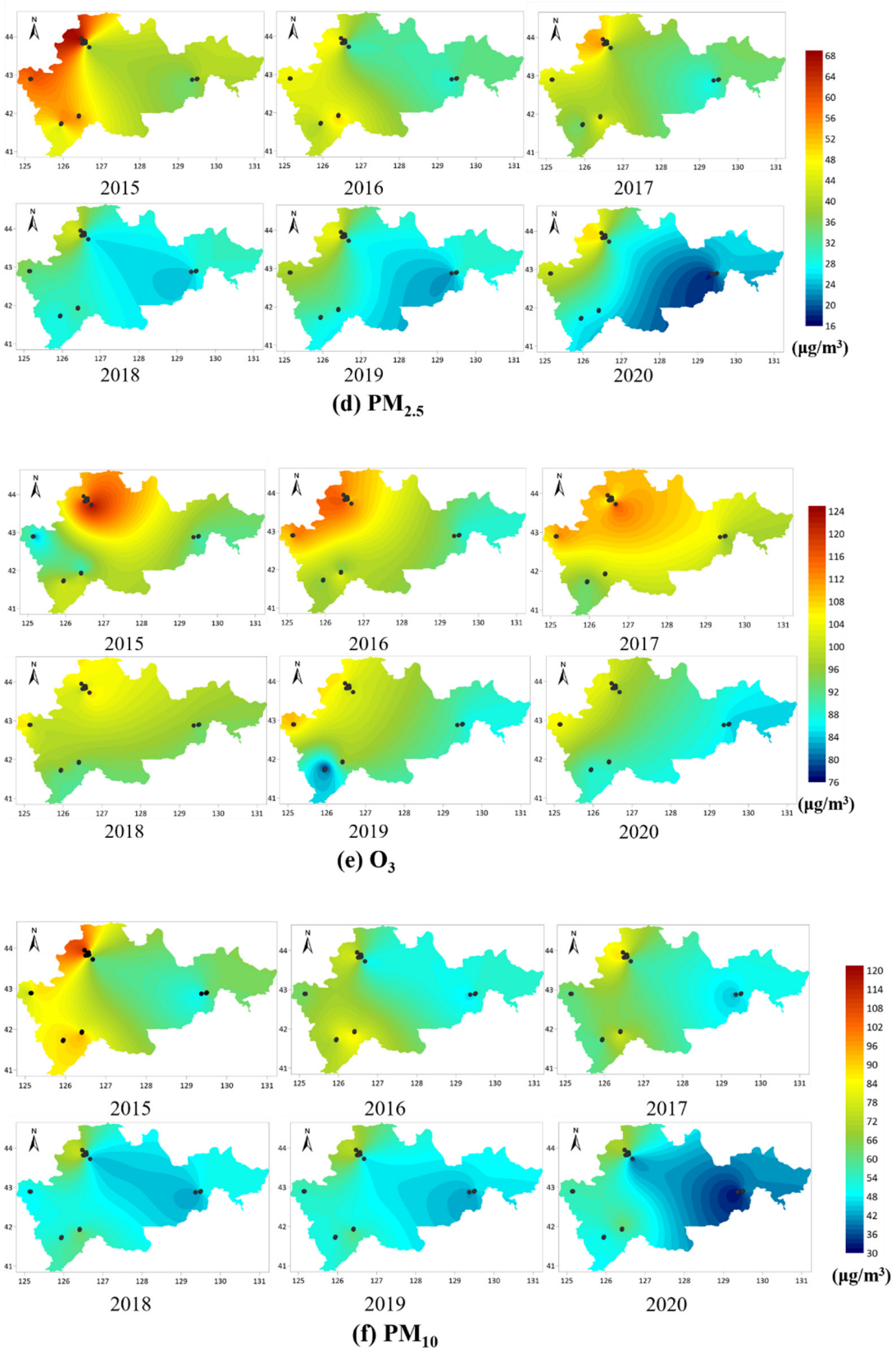

Figure 3. Spatial distribution of annual average concentrations of six pollutants in the eastern Jilin Province, China, from 2015 to 2020. (**a**) CO unit: mg/m^3; (**b**) SO_2 unit: μg/m^3; (**c**) NO_2 unit: μg/m^3; (**d**) $PM_{2.5}$ unit: μg/m^3; (**e**) O_3 unit: μg/m^3; (**f**) PM_{10} unit: μg/m^3. (The black dot on the figure is the position of the monitoring point).

We used the Ward1 method in SPSS to cluster 16 monitoring points, and the results are shown in Figure 4. We found a fascinating phenomenon: most sites complied with the spatial distribution results, but JL6 and JL7 sites were always not crowded with other JL sites. The JL7 site was notable because the JL7 site was located at the northernmost end of Jilin City. It is an emerging industrial park. More than a dozen large and small chemical enterprises are in the park, which led to JL7 being divided into one category alone. Taking the cluster analysis of $PM_{2.5}$ as an example, the JL6 site was not classified with other JL sites but with the YB1-3 sites. This was because the JL6 site was located in the tourist area of Jilin City, only surrounded by some sanatoriums and a small number of residential areas. Its south was Songhua Lake's scenic spot. As shown in Figure 2, the JL6 site was a scenic spot in Jilin City. It is subject to more strict pollutant control and has no industrial emissions and severe traffic pollution. Therefore, the concentration of various pollutants was low, resulting in the specific particularity of the JL6 site and clustering with the YB site with the same low pollutant concentration.

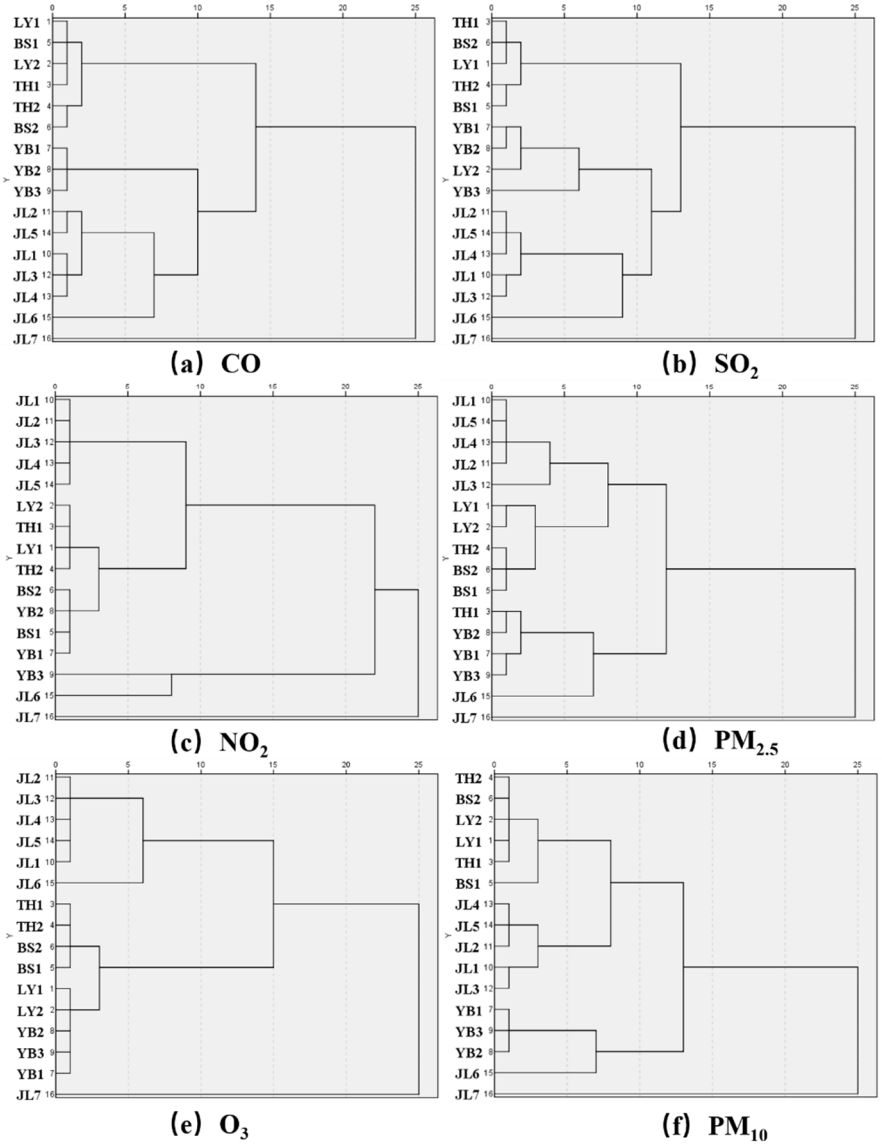

Figure 4. Cluster analysis of 16 monitoring stations based on pollutant concentration. (**a**) CO; (**b**) SO_2; (**c**) NO_2; (**d**) $PM_{2.5}$; (**e**) O_3; (**f**) PM_{10}.

Figure 5 shows the five-year concentration changes in six conventional pollutants. The annual O_3 average was calculated using the daily O_3 maximum, and the yearly average of

other pollutants was computed using all hourly data. It can be found that the six pollutants generally showed a decreasing trend year by year. The concentrations of NO_2 and CO reached the lowest in 2020, which were 20.87 μg/m^3 and 0.77 mg/m^3, respectively. This was due to lockdowns caused by the novel coronavirus pneumonia in the first half of 2020, a sudden decrease in vehicle flow, and a reduction in emissions, resulting in a decrease in the concentration of the two pollutants. The SO_2 concentration decreased year by year and rose to some extent in 2020. From 2015 to 2020, the SO_2 concentration at all stations decreased by 50.52% on average. From 2015 to 2020, the average annual concentration of NO_2 at all stations decreased by 31.11%. It is speculated that the change in SO_2 and NO_2 was due to the reduction in coal consumption and the reduction in pollutant emissions due to the implementation of central heating and the replacement of small boilers in Northeast China in recent years. Similarly, after Krakow promulgated the law banning the use of solid fuels, local air pollution was significantly alleviated [10]. PM_{10} and $PM_{2.5}$ decreased significantly in 2016, increased slightly in 2017, and then continued to decrease. The significant reduction in particulate matter in 2016 is related to continuous precipitation in autumn 2016. Rainwater caused a large amount of particulate matter to settle into the ground through wet sedimentation to purify the air. The increase in particulate matter concentration in 2017 was due to the lack of strict control over straw incineration, resulting in the recovery of fine particulate matter concentration. In 2018, a strict straw burning ban policy was implemented in the east of Jilin Province, which reduced the mass concentration of particulate matter to a certain extent. This finding was consistent with other studies on straw incineration in Jilin Province [31]. The annual average concentration of CO was similar to that of PM_{10} and $PM_{2.5}$, which increased first and then decreased. There was little difference in the average concentration of O_3 in each year. The O_3 concentration of BS2, YB1, YB2, YB3, JL1, and LY1 increased, while it decreased at other stations. Among them, the concentration of JL1 increased by 17.29%, and that of JL6 decreased by 20.99%. Among the six pollutants, only the concentration of O_3 rose greatly in some stations.

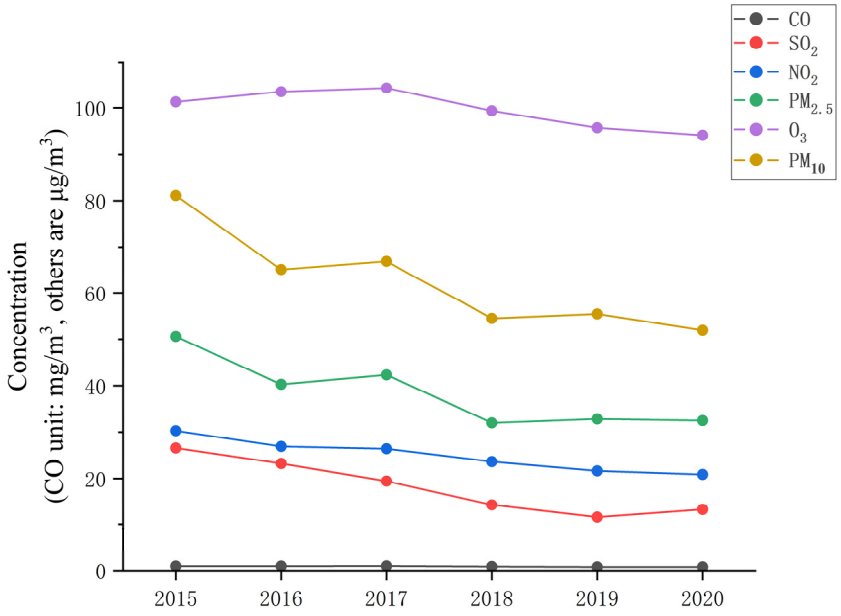

Figure 5. Change trend in annual average concentrations of six pollutants (CO, SO_2, NO_2, O_3, $PM_{2.5}$, PM_{10}) in the eastern Jilin Province, China, from 2015 to 2020 (CO unit: mg/m^3, others are μg/m^3).

3.1.2. Seasonal and Hourly Variation of Pollutant Concentration

Figure 6 shows the seasonal changes in the concentrations of six pollutants in the eastern region of Jilin Province from 2015 to 2020. We can see from the figure that the seasonal variation of pollutant concentration in the study area is very significant. Except for O_3 pollution, which was the most serious in spring, the concentration of the other five

pollutants was the highest in winter. The highest concentration of pollutants occurred at 7:00–10:00 and 18:00–21:00. Overall, O_3 pollution was the most serious in spring, followed by summer. O_3 pollution in autumn and winter was significantly lower than that in other seasons. The lower O_3 concentration in winter might be since the radiation level in winter was lower than in other seasons. The lack of light and low temperature in winter was not conducive to O_3 formation, while a large amount of O_3 was generated when the solar radiation increased in spring [32].

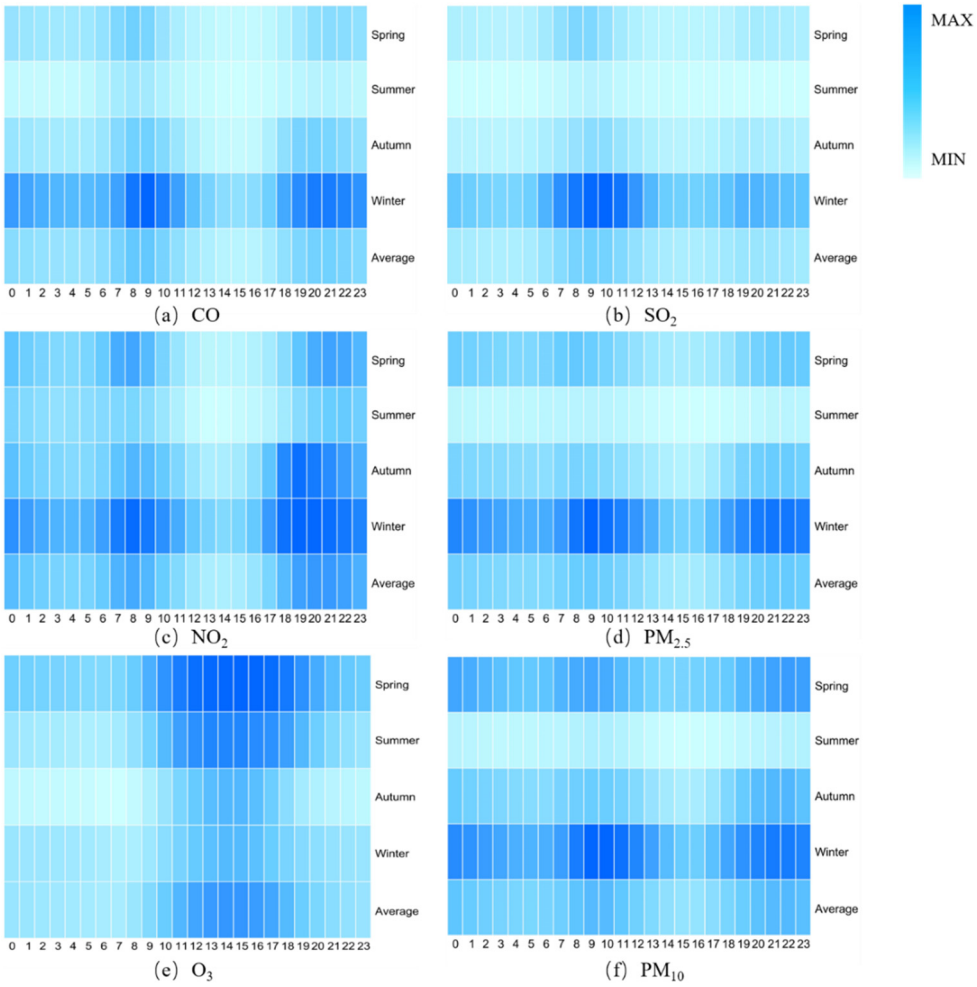

Figure 6. Hourly variation of six pollutant concentrations in different seasons from 2015 to 2020. (**a**) CO; (**b**) SO_2; (**c**) NO_2; (**d**) $PM_{2.5}$; (**e**) O_3; (**f**) PM_{10}. (The CO concentration range is 0.65–1.46 mg/m^3. The SO_2 concentration range is 7.27–51.99 μg/m^3. The NO_2 concentration range is 11.35–39.92 μg/m^3. The $PM_{2.5}$ concentration range is 16.08–75.31 μg/m^3. The O_3 concentration range is 27.97–120.63 μg/m^3. The PM_{10} concentration range is 30.31–101.78 μg/m^3).

The concentrations of $PM_{2.5}$, PM_{10}, and SO_2 were winter > spring > autumn > summer, which was consistent with the seasonal changes shown in other regions [33]. In spring, summer, and autumn, the hourly concentration was higher from 7:00 to 9:00, and the concentration was relatively low from 12:00 to 18:00. In winter, the concentrations of the three pollutants were relatively low from 15:00 to 16:00. For PM_{10} and $PM_{2.5}$, there were two high values throughout the year; one was in spring with frequent dust weather, and the other was in winter after the beginning of the heating period. Especially after entering the heating period, the mass concentrations of $PM_{2.5}$ and PM_{10} increased sharply, indicating that fossil energy consumption contributed greatly to the mass concentration of particulate matter. At the same time, the open burning of straw in autumn and winter before 2018 also led to the increase in particulate pollution [34]. At 9:00 in winter and at night, there was

more particulate severe pollution, similar to that in autumn. The reason for this pollution was mainly caused by the heating period, adverse temperature, and other meteorological conditions that were not conducive to the dilution of pollutants [35]. There was no significant difference in SO_2 pollution between spring and autumn, and the difference in average concentration between winter and summer was as high as 25.73 $\mu g/m^3$. The sharp increase in SO_2 concentration in winter was mainly due to the large amount of coal consumption for heating in winter, which released a large amount of SO_2. In addition, the cold winter in northern China and adverse meteorological conditions made SO_2 unable to be diluted.

The concentration of NO_2 was winter > autumn > spring > summer, which was consistent with the relevant research results [36], and the concentration in winter was significantly higher than that in summer. The period with low NO_2 concentration occurred from 13:00 to 17:00. The high concentration in winter might have been due to the cold winter in the study area and the increase in coal consumption for heating, increasing NO_2 concentration. CO pollution was light in spring, summer, and autumn, and there was little difference between seasons. Its mass concentration in winter was significantly higher than that in other seasons. The severe pollution in winter might have been due to the influence of temperature inversion in winter, which made CO unable to be diluted, increasing pollutant concentration. In summer, the atmospheric convection activity was vigorous and accelerated the dilution of pollutants. The high-value period of CO and NO_2 concentration was in the traffic peak period from 7:00 to 9:00 and 19:00 to 22:00. The vehicle exhaust pollution generated by people's travel was the primary source of these two pollutants. However, the contaminants were not diluted in time due to adverse meteorological conditions in winter, resulting in the concentration of CO and NO_2 in winter being significantly higher than that in other seasons.

To further analyze the hourly variation trend of pollutants, we separated 16 monitoring stations according to cities to explore the hourly variation. This study used the mass concentrations of six conventional pollutants from 2 January 2015, to 31 December 2020, from 16 air quality monitoring stations. The results are shown in Figure 7.

The hourly variation in O_3 in the five towns was highly similar. The daily high-value area of O_3 appeared at 14:00–17:00, and the low-value site appeared at 6:00–8:00. The high value of O_3 in the afternoon was because many O_3 precursors accumulated in transportation during the day. The temperature was the highest in the afternoon, and solar radiation was the strongest, resulting in much O_3 generation. When solar radiation could not maintain a photochemical reaction at night, O_3 was mainly removed through the titration reaction of $O_3 + NO \rightarrow NO_2 + O_2$, resulting in the decrease in O_3 concentration at night. Consistent with the spatial distribution diagram shown in Figure 3, the O_3 concentration at the JL site was the highest, while that at BS and TH sites was low.

The hourly concentration changes in CO and NO_2 in the five cities were also very similar, showing a "double peak" trend. The two peaks were at the peak of traffic, 7:00–9:00 and 18:00–21:00, respectively. SO_2 levels reached the maximum at 9:00, and the maximum SO_2 values of BS and TH were 41.76 $\mu g/m^3$ and 41.61 $\mu g/m^3$, respectively. The peak value of SO_2 in these two cities was 14–23 $\mu g/m^3$ higher than in other cities, which is a considerable gap. The increase in SO_2 concentration was due to the exhaust emission of motor vehicles, so the SO_2 concentration increased in five areas during the peak traffic period. However, TH and BS belong to basin terrain, the climate was relatively stable, and the pollutants were not easy to dilute, resulting in high SO_2 concentrations. SO_2 also had a small peak at night, which may be related to the restriction of large diesel trucks during the day, making large trucks appear at night [37]. The first peak of NO_2 occurred from 7:00 to 8:00, and the late height was between 19:00 and 21:00. The first peak was caused by the fact that the NO emitted by motor vehicles reacts with free radicals to produce a large amount of NO_2. The rise at night was mainly due to the titration reaction between NO emitted by motor vehicles and O_3 to make NO_2.

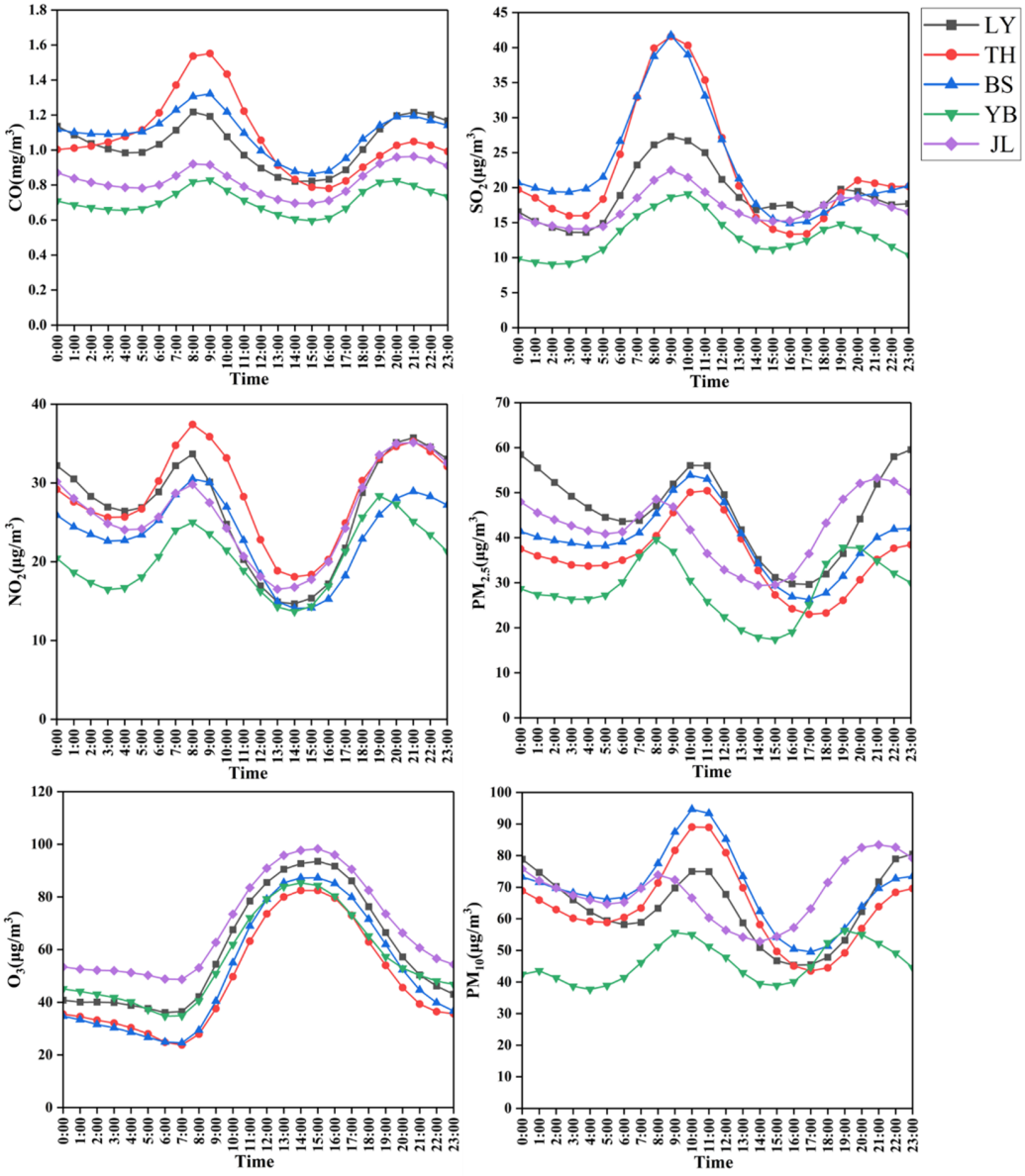

Figure 7. Hourly variation of six pollutant concentrations in different cities.

The hourly changes in $PM_{2.5}$ and PM_{10} were very similar. According to the peak time of pollutants, cities were divided into two categories: YB and JL were one category, and the other three cities were classified into another category. The peaks of LY, TH, and BS appeared from 9:00 to 11:00, reached the valley value from 17:00 to 18:00, and entered the second high-value area at 22:00. The morning peaks of YB and JL appeared at 8:00–9:00, which was speculated to be related to the increase in human activities during this period [38]. Then, the concentration showed a downward trend. After falling to the valley value around 15:00–16:00, the concentration began to rise, and the second high-value area was between 17:00 and 21:00. The hourly variation law of $PM_{2.5}$ of YB and JL was consistent with the research in Beijing. The concentration at night was higher than that during the day [39]. The peak time of TH, BS, and LY was consistent with that in other parts of China [40]. The reason why the $PM_{2.5}$ peak of YB and JL appeared in advance may be related to human activities, such as the difference in people's travel mode and commuting time, which needs further research.

At the same time, the concentrations of CO, NO_2, $PM_{2.5}$, and PM_{10} rose slightly in the evening. This was because the temperature decreased in the evening, the boundary layer (BL) dropped with cooling, and the aerosol, dust, gas, and any other mixture released

from the ground source were blocked in the BL to a great extent. This led to the increase in pollutant concentration at night [41].

3.1.3. Monthly Variation of Pollutant Concentration

The concentration stack diagram is used to describe the contribution of six pollutants to pollution in other months. The results are shown in Figure 8. Through the superposition of absolute concentrations of contaminants, we intuitively found that the monthly breakdown in the study area presented a "U" distribution. The pollution was most serious in January, followed by February, March, April, and December, and less so in July, August, and September. Except for O_3, the monthly concentrations of the other five pollutants were consistent with the total pollution trend, showing a "U" distribution.

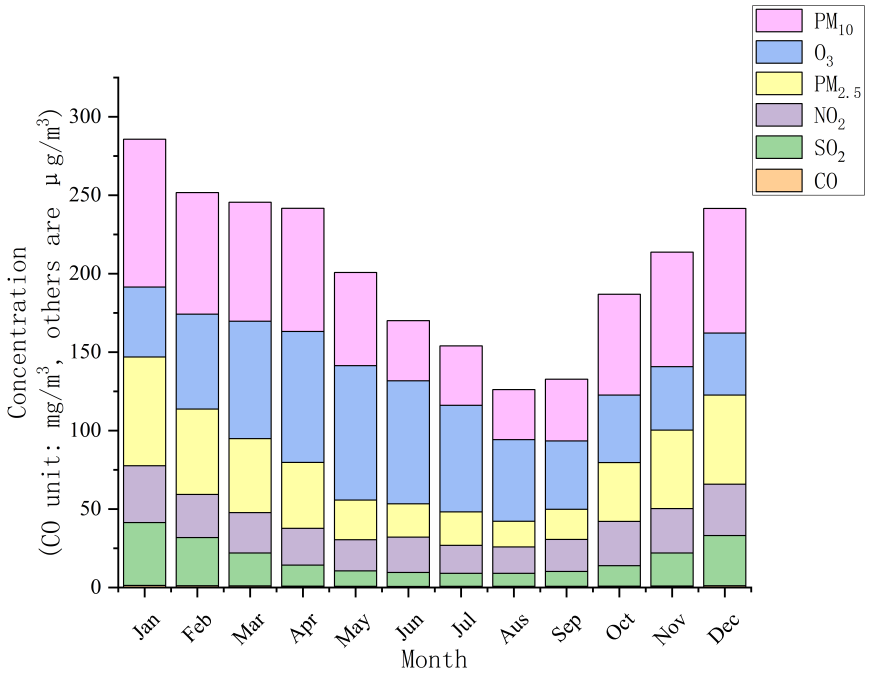

Figure 8. Monthly variation of six pollutant concentrations from 2015 to 2020 (CO unit: mg/m^3, others are μg/m^3).

On the contrary, O_3 showed an "n" trend. The O_3 concentration was the highest in April, May, and June and the lowest in January, February, October, November, and December. The concentration of O_3 was the highest in May because of the long illumination time, intense solar radiation, and high temperature in May. PM_{10} and $PM_{2.5}$ were high in January, February, March, November, and December, and low in July, August, and September. SO_2 pollution was the most serious in January, February, and December, and light in July and August. The high-value area of NO_2 was distributed from January to March and from October to December, with the highest in January and the lowest in August. The increase in SO_2, NO_2, $PM_{2.5}$, and PM_{10} in winter was caused by coal-fired heating. The air quality improved greatly in July and August because the increase in rainfall inhibited the transport of pollutants and accelerated the deposition of pollutants. CO pollution was the most serious in January (1.29 mg/m^3) and the least serious in June (0.69 mg/m^3). There was no significant difference in concentration between different months. These results are consistent with the seasonal changes above.

3.2. Backward Trajectory Cluster Analysis

Considering that JL is the most economically developed and seriously polluted area among the five cities in the eastern part of Jilin Province, and JL1 monitoring point (126.555 E, 43.8875 N) was located in the center of Jilin City, which is the industrial concentration area and transportation hub of Jilin City, with many surrounding pollution sources.

Therefore, we used the HYSPLIT model to cluster 8760 trajectories passing through the JL1 monitoring point in 2019 and calculate the proportion of various trajectories in the total trajectories. The results are shown in Figure 9 and Table 3. We further analyzed the trajectory and subdivided it into four seasons: spring, summer, autumn, and winter for trajectory clustering. Observe the difference in airflow transport in different seasons. The results are shown in Figure 10. It is found that the track with the most significant proportion was the track of Korea Liaoning Province in the southwest, accounting for 37.94% (cluster 2), and the track transportation distance was the shortest. The path passing through Inner Mongolia and Heilongjiang Province in the northwest accounted for the second largest, reaching 27.38% (cluster 4). In addition, there were two track clusters in the northwest, the circulation track of Russia and Inner Mongolia accounts for 18.11% (cluster 3), and the most extended track cluster passed through Russia and Mongolia, accounting for 16.57% (cluster 1). In conclusion, the pollutants were mainly affected by the airflow from the northwest and southwest.

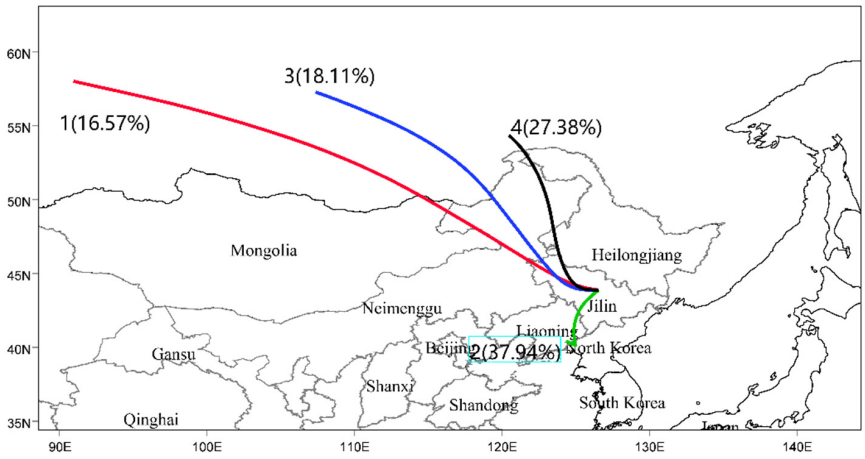

Figure 9. Cluster distribution of backward trajectory in 2019. The trajectories are divided into four clusters: cluster 1 is in red; cluster 2 is in green; cluster 3 is in blue; cluster 4 is in black.

Table 3. Backward trajectory clustering results.

Cluster	Direction	Pathway Region	Probability of Occurrence (%)
1	Northwest	Russia, Mongolia, Neimenggu	16.57
2	Southwest	Liaoning Province, North Korea	37.94
3	Northwest	Russia, Mongolia, Neimenggu	18.11
4	North by West	Russia, Neimenggu, Heilongjiang Province	27.38

Figure 10 shows the trajectory clustering results of four spring, summer, autumn, and winter seasons in eastern Jilin Province in 2019. We found that the trajectory had prominent seasonal characteristics. The clustering results in spring and autumn were similar to those in the whole year, mainly affected by the long-distance transmission in Northwest China and the short-distance transmission in Southwest China. The trajectory cluster in summer was the most special in the four seasons. In addition, the northwest cluster (Russia–Mongolia–Inner Mongolia) was also affected by the southeast ocean circulation, accounting for 8.7%. In summer, the trajectory from the southwest was the Yellow Sea Liaoning sea–land breeze circulation, accounting for 51.47%. The more complex airflow in summer might provide great help for the dilution of pollutants, resulting in the generally low concentration of contaminants in summer. In winter, it was mainly affected by long-distance transportation in the northwest (Russia–Mongolia–Inner Mongolia), and the track transmission distance was the longest, accounting for 47.71%.

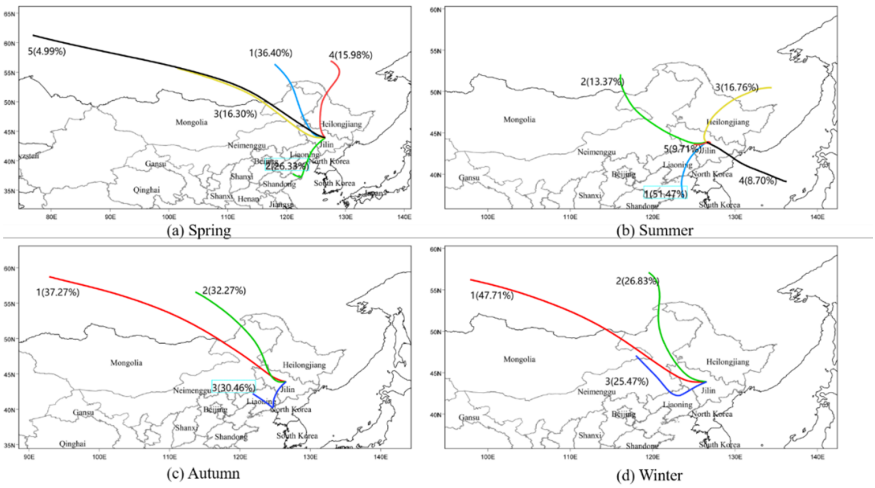

Figure 10. The trajectory clustering results of four spring, summer, autumn, and winter seasons in eastern Jilin Province in 2019. In (**a**), the trajectories are divided into five clusters: cluster 1 is in blue; cluster 2 is in green; cluster 3 is in yellow; cluster 4 is in red; cluster 5 is in black. In (**b**), the trajectories are divided into five clusters: cluster 1 is in blue; cluster 2 is in green; cluster 3 is in yellow; cluster 4 is in black; cluster 5 is in red. In (**c**,**d**), the trajectories are divided into three clusters: cluster 1 is in red; cluster 2 is in green; cluster 3 is in blue.

Moreover, the other two tracks in winter also came from the northwest. In other words, in winter, almost all airflow went from the northwest. Therefore, we must strengthen international and regional joint prevention and control of air pollution in the northwest.

3.3. Analysis of Potential Pollution Sources

The potential sources of $PM_{2.5}$ at the JL1 monitoring point in 2019 were analyzed, and the results of WPSCF and CWT are shown in Figures 11 and 12. It can be seen that the WPSCF high-value area of $PM_{2.5}$ was the northwest and southeast regions. The WPSCF value in the northwest was high, mainly concentrated in Russia, Mongolia, and Inner Mongolia, reaching 0.9–1. There were also a few high-value areas in Liaoning Province in the southwest, with WPSCF values ranging from 0.9 to 1. In addition, there were a few high-value areas in the southeast, with a WPSCF value > 1. However, the potential contribution source area in the northwest was much larger than in the southwest and southeast. $PM_{2.5}$ in the study area was mainly affected by northwest airflow, southwest airflow, and a small part of southeast airflow. The WPSCF values in other regions were primarily between 0.1 and 0.7. According to the results of CWT, the high-value area of $PM_{2.5}$ potential source was distributed in the northwest, which was consistent with the results of WPSCF.

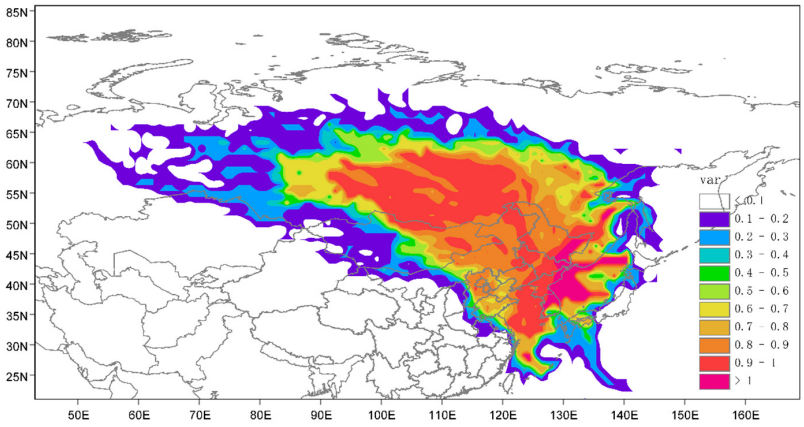

Figure 11. Weighted potential source contribution function (WPSCF) values for $PM_{2.5}$.

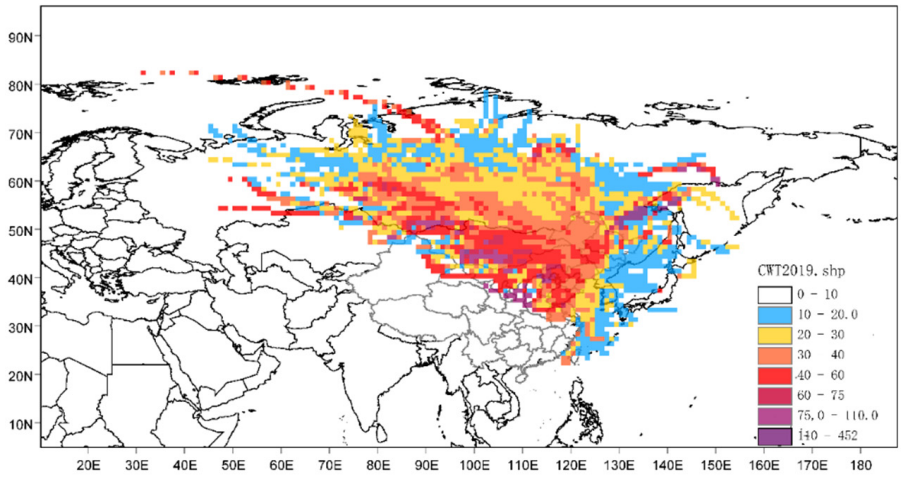

Figure 12. Concentration trajectory weighting method (CWT) values for $PM_{2.5}$.

3.4. Analysis of Weekend Effect of CO, NO_2, $PM_{2.5}$ and O_3

The WEs of CO, NO_2, $PM_{2.5}$, and O_3 at each station from 2016 to 2019 are shown in Figure 13. We can see that O_3 in most stations presented a "negative weekend effect" in 2016 and 2017, indicating that the average concentration on weekends was slightly lower than that on weekdays. O_3 became a "positive weekend effect" in 2018 and 2019, which was opposite to the change in the weekend effect of NO_2. This was different from many studies. Seguel, R.J, and others found that the O_3 concentration in Santiago, Chile, on weekends was higher than on weekdays, showing a positive weekend effect [42]. Tang et al. found that the positive weekend effect in Shanghai was due to nitrogen oxides and the photochemical reaction ratio [43]. Atkinson Palombo et al. showed that the weekend effect might be caused by other variables affecting O_3 (such as temperature, solar radiation, PM_{10}, and relative humidity) in a specific location [44]. Zou, e, and others found that the weekend effect of O_3 mainly depended on anthropogenic emissions on O_3 precursors and was related to non-methane hydrocarbons [45]. The reasons for the "negative weekend effect" of O_3 in the eastern part of Jilin Province were complex. We speculate that the reason was that the traffic flow on weekends was lower, and the NO_x emission was not as strong as that on weekdays, resulting in the weakening of the titration reaction of $O_3 + NO \rightarrow NO_2 + O_2$ and the increase in O_3 concentration on weekends. Meanwhile, the weekend effect of $PM_{2.5}$ in 2019 was negative, indicating that the weekend $PM_{2.5}$ concentration was lower than that on weekdays. The reduction in aerosol emissions led to stronger solar radiation, which increased the weekend O_3 concentration, showing a positive weekend effect [46].

For $PM_{2.5}$, all stations showed a "positive weekend effect" in 2016, and the intensity of positive weekend effect decreased year by year from 2016, and most stations showed a "negative weekend effect" by 2019. For NO_2 and CO, TH1, TH2, YB1, YB2, and YH3 stations showed a noticeable positive weekend effect from 2016 to 2018. It may be that these stations are located in tourist cities in the east of Jilin Province, and the enormous traffic flow on weekends and other holidays led to the increase in NO_2 and CO emissions. For the JL1–7 stations, NO_2 gradually changed from a "positive weekend effect" to a "negative weekend effect," which might be due to the large truck traffic on weekdays in Jilin City, a vital old industrial base, and a chemical city in Northeast China.

According to the cumulative diagram of the interannual variation deviation of weekend effect (Figure 14), it is found that the deviation of the "weekend effect" of pollutants showed a decreasing trend and showed a trend of changing from "positive weekend effect" to "negative weekend effect" on the whole. This is not the first time that a decreasing trend of the "weekend effect" has been found. Wang Yuzhen and others analyzed $PM_{2.5}$ in 338 cities in China and found that $PM_{2.5}$ had no noticeable weekend effect from 2014 to 2017. George t et al. analyzed the O_3 data from 1997 to 1999 and found that the "weekend effect"

was evident in many cities. Still, the O_3 data from 2008 to 2010 showed that this phenomenon disappeared [47]. The decrease in "weekend effect" may be related to the change in people's production and lifestyle. However, the influencing factors of the "weekend effect" are too complex and depend on the chemical status characteristics of each city. Therefore, further research is still needed to determine the reasons for the reduction in the "weekend effect" .

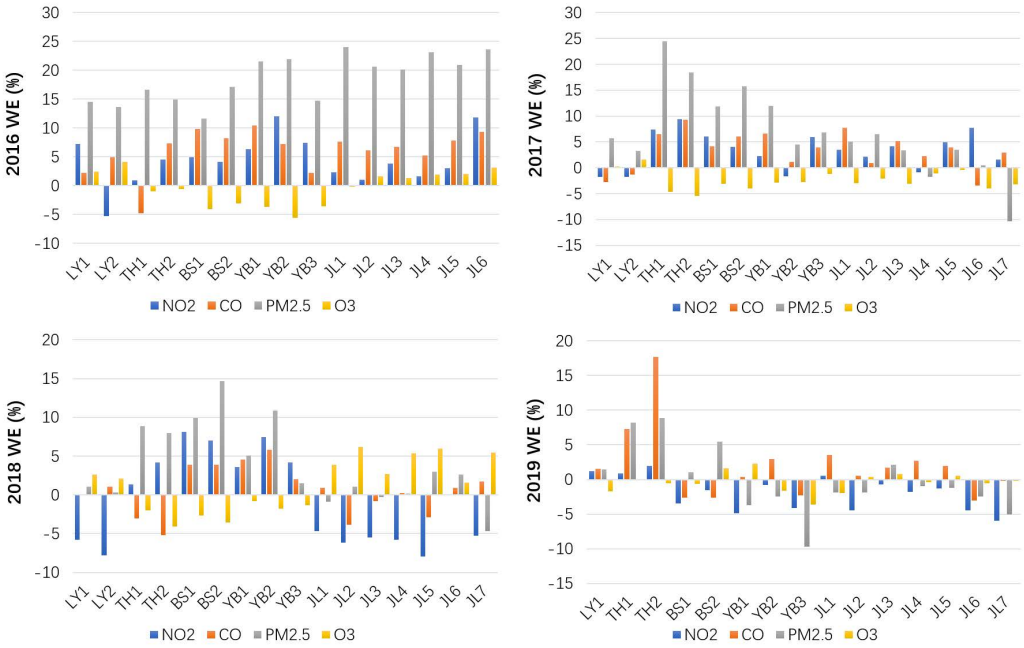

Figure 13. Weekend effect index of four pollutants at each station in 2016–2019.

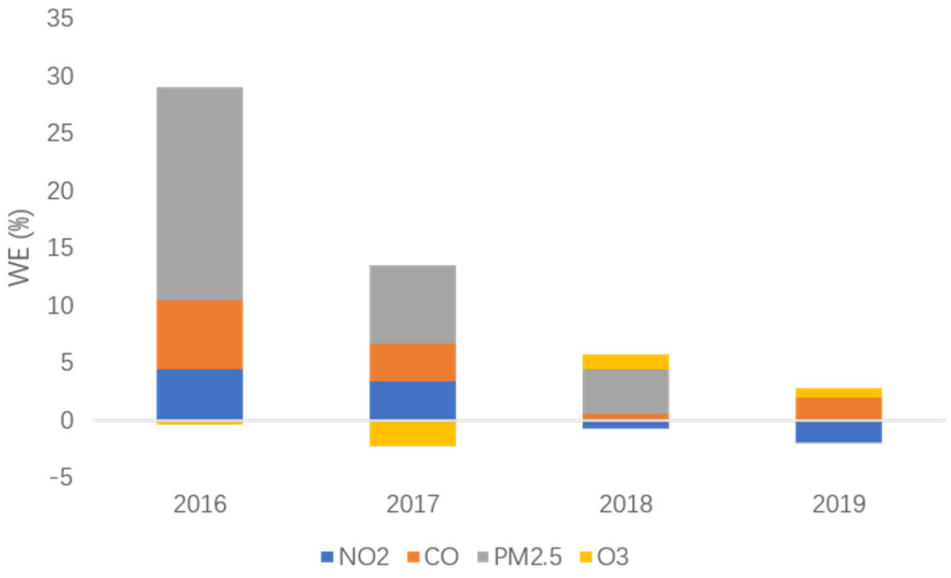

Figure 14. Cumulative diagram of inter-annual variation deviation of weekend effect.

4. Conclusions

By analyzing the temporal and spatial distribution of six pollutants, this paper comprehensively understood the atmospheric environmental quality in the east of Jilin Province. Overall, the air quality in the study area improved year by year. However, the pollutant concentration still exceeded the standard in some areas, and the pollutant concentration had prominent geographical characteristics. At the same time, pollutants had obvious seasonal characteristics related to coal-fired heating in autumn and winter. The results

of backward trajectory analysis showed that the potential pollution source areas of $PM_{2.5}$ were located in the northwest and southwest, indicating that strengthening regional joint governance is essential to improve air quality. Through the analysis of the weekend effect, it was found that the concentration of pollutants is indeed related to human activities. The research results of this paper can provide an excellent theoretical basis for the prevention and control of air pollution in the eastern part of Jilin Province.

(1) The concentrations of O_3, PM_{10}, and $PM_{2.5}$ were higher in northwest Jilin, while the concentrations of SO_2 and CO were higher in southwest Jilin. On the whole, the six pollutants showed a decreasing trend year by year. The O_3 concentration of some stations rebounded considerably. The amount of SO_2 and NO_2 decreased during the COVID-19 lockdowns in 2020. That shows that stricter laws and procedures play an essential role in improving regional pollution. China has not yet issued a special decree on straw incineration treatment, which does not match the urgent straw treatment demand in Northeast China. Therefore, it is suggested to speed up the formulation process of straw governance laws and improve air quality. Motor vehicle exhaust was a fundamental reason for the increase in SO_2 and NO_2 concentrations. Therefore, urban public transport facilities can be improved and motor vehicle exhaust emissions can be reduced from the source.

(2) The seasonal difference in O_3 concentration was spring > summer > winter > autumn, NO_2 was winter > autumn > spring > summer, SO_2, PM_{10}, and $PM_{2.5}$ were winter > spring > autumn > summer, CO concentration was low throughout the year, and there was little change between seasons. The pollution was the most serious in January, followed by February and March, and the pollution was mild in July, August, and September. PM_{10} and $PM_{2.5}$ showed highly similar variation characteristics among the hourly variation characteristics, indicating that PM_{10} in the study area contains $PM_{2.5}$, and $PM_{2.5}$, and PM_{10} that can be managed together. The concentration of SO_2 at 8:00–10:00 at BS and TH stations was exceptional. The concentration of SO_2 at BS and TH stations was exceptional, and the peak value was 14–23 $\mu g/m^3$ higher than that in other cities. Because TH and BS belong to basin terrain, there was much calmer weather, and the pollutants were not easy to be diluted, so the SO_2 concentration was high during peak traffic hours. Therefore, the air quality can be improved by introducing single and double traffic restrictions, improving public transport equipment, and improving fuel quality.

(3) The study area was mainly affected by airflow pathways in northwest and southwest directions. The WPSCF high-value areas of $PM_{2.5}$ are mainly in the northwest and southwest, and a small part of the high-value areas are in the southeast. As the study area was located at the border of China and has a long track from the northwest, it is essential to strengthen inter-regional joint governance.

(4) O_3 showed a negative weekend effect in 2016 and 2017 and became a positive weekend effect in 2018 and 2019, which was opposite to the weekend effect of NO_2. The change in the O_3 weekend effect from negative to positive was mainly due to the weakening of the $O_3 + NO \rightarrow NO_2 + O_2$ titration reaction due to low weekend traffic flow. $PM_{2.5}$ gradually changed from a "positive weekend effect" to a "negative weekend effect". For NO_2 and CO, sites in tourist cities showed an obvious "positive weekend effect". The monitoring point NO_2 in the chemical city gradually changed from a "positive weekend effect" to a "negative weekend effect". According to the cumulative diagram of the inter-annual variation deviation of the weekend effect, it was found that the deviation of pollutant "weekend effect" gradually decreased. Further research is still needed to determine the reasons for the reduction in the "weekend effect". However, the analysis of this paper still has several limitations. For example, the distribution of monitoring points was uneven, and the number was limited, which might mean that the monitoring concentration may not accurately represent the whole region.

Supplementary Materials: The following supporting information can be downloaded at: https://www.mdpi.com/article/10.3390/atmos13050681/s1. Table S1: Details of Eastern Jilin Province.; Table S2: Main economic activities in Eastern Jilin Province in 2020.

Author Contributions: Data curation and methodology, J.W.; supervision and validation, C.F.; conceptualization, original draft writing, review and editing, K.X.; formal analysis, J.L. All authors have read and agreed to the published version of the manuscript.

Funding: This research received no external funding.

Institutional Review Board Statement: Not applicable.

Informed Consent Statement: Not applicable.

Data Availability Statement: Not applicable.

Acknowledgments: The authors would like to thank the group members of Laboratory 537 and 142 of Jilin University.

Conflicts of Interest: The authors declare no conflict of interest.

References

1. Hu, F.; Guo, Y. Health impacts of air pollution in China. *Front. Environ. Sci. Eng.* **2021**, *15*, 74. [CrossRef]
2. Liu, S. Analysis of Soil Aeolian Dust Composition Spectrum and Environmental Risk Assessment of Heavy Metals in Luliang City. Master's Thesis, Taiyuan University of Technology, Taiyuan, China, 2015.
3. Li, Q. Study on Temporal and Spatial Distribution Characteristics and Influencing Factors of Ozone Concentration in Shenyang. Master's Thesis, Shenyang University of Aeronautics and Astronautics, Shenyang, China, 2019.
4. Cheng, L.; Wang, S.; Gong, Z.; Yang, Q.; Wang, Y. Ozone pollution trend and temporal and spatial distribution characteristics in Beijing Tianjin Hebei region. *Environ. Monit. China* **2017**, *33*, 14–21.
5. Li, T.; Yan, M.; Ma, W.; Ban, J.; Liu, T.; Lin, H.; Liu, Z. Short-term effects of multiple ozone metrics on daily mortality in a megacity of China. *Environ. Sci. Pollut. Res.* **2015**, *22*, 8738–8746. [CrossRef]
6. Feng, Z.; Hu, E.; Wang, X.; Jiang, L.; Liu, X. Ground-level O3 pollution and its impacts on food crops in China: A review. *Environ. Pollut.* **2015**, *199*, 42–48. [CrossRef]
7. Monks, P.S.; Archibald, A.T.; Colette, A.; Cooper, O.; Coyle, M.; Derwent, R.; Fowler, D.; Granier, C.; Law, K.S.; Mills, G.E.; et al. Tropospheric ozone and its precursors from the urban to the global scale from air quality to short-lived climate forcer. *Atmos. Chem. Phys.* **2015**, *15*, 8889–8973. [CrossRef]
8. Li, X.; Song, J.; Lin, T.; Dixon, J.; Zhang, G.; Ye, H. Urbanization and health in China, thinking at the national, local and individual levels. *Environ. Health* **2016**, *15*, S32. [CrossRef]
9. Cao, D.; Ramirez, C.D. Air Pollution, Government Pollution Regulation, and Industrial Production in China. *J. Syst. Sci. Complex.* **2020**, *33*, 1064–1079. [CrossRef]
10. Danek, T.; Zaręba, M. The Use of Public Data from Low-Cost Sensors for the Geospatial Analysis of Air Pollution from Solid Fuel Heating during the COVID-19 Pandemic Spring Period in Krakow, Poland. *Sensors* **2021**, *21*, 5208. [CrossRef]
11. Meng, C.; Tang, Q.; Yang, Z.; Cheng, H.; Li, Z.; Li, K. Collaborative control of air pollution in the Beijing–Tianjin–Hebei region. *Environ. Technol. Innov.* **2021**, *23*, 101557. [CrossRef]
12. Wang, L.; Zhang, F.; Pilot, E.; Yu, J.; Nie, C.; Holdaway, J.; Yang, L.; Li, Y.; Wang, W.; Vardoulakis, S.; et al. Taking Action on Air Pollution Control in the Beijing-Tianjin-Hebei (BTH) Region: Progress, Challenges and Opportunities. *Int. J. Environ. Res. Public Health* **2018**, *15*, 306. [CrossRef]
13. Wang, L.; Xiong, Q.; Wu, G.; Gautam, A.; Jiang, J.; Liu, S.; Zhao, W.; Guan, H. Spatio-Temporal Variation Characteristics of PM2.5 in the Beijing–Tianjin–Hebei Region, China, from 2013 to 2018. *Int. J. Environ. Res. Public Health* **2019**, *16*, 4276. [CrossRef] [PubMed]
14. Li, H.; Song, Y.; Zhang, M. Study on the gravity center evolution of air pollution in Yangtze River Delta of China. *Nat. Hazards* **2017**, *90*, 1447–1459. [CrossRef]
15. Song, Y.; Liu, B.; Chen, X.; Liu, J. Liu Atmospheric Pollution Mapping of the Yangtze River Basin: An AQI-Based Weighted Co-Word Analysis. *Int. J. Environ. Res. Public Health* **2020**, *17*, 817. [CrossRef] [PubMed]
16. Kong, L.; Hu, M.; Tan, Q.; Feng, M.; Qu, Y.; An, J.; Zhang, Y.; Liu, X.; Cheng, N. Aerosol optical properties under different pollution levels in the pearl river delta (PRD) region of China. *J. Environ. Sci.* **2021**, *104*, 182–187. [CrossRef] [PubMed]
17. Ministry of Ecology and Environment of the People's Republic of China. *HJ/T193-2005, Monitoring Regulation for Ambient Air Quality*; China Environmental Science Press: Beijing, China, 2005.
18. Rühaak, W. 3-D interpolation of subsurface temperature data with measurement error using kriging. *Environ. Earth Sci.* **2015**, *73*, 1893–1900. [CrossRef]
19. Murtagh, F.; Legendre, P. Ward's Hierarchical Agglomerative Clustering Method: Which Algorithms Implement Ward's Criterion? *J. Classif.* **2014**, *31*, 274–295. [CrossRef]

20. Sun, J.; Huang, L.; Liao, H.; Li, J.; Hu, J. Impacts of Regional Transport on Particulate Matter Pollution in China: A Review of Methods and Results. *Curr. Pollut. Rep.* **2017**, *3*, 182–191. [CrossRef]
21. Fang, C.; Gao, J.; Wang, D.; Wang, D.; Wang, J. Optimization of stepwise clustering algorithm in backward trajectory analysis. *Neural Comput. Appl.* **2020**, *32*, 109–115. [CrossRef]
22. Liu, B.; Song, N.; Dai, Q.; Mei, R.; Sui, B.; Bi, X.; Feng, Y. Chemical composition and source apportionment of ambient PM2.5 during the non-heating period in Taian, China. *Atmos. Res.* **2016**, *170*, 23–33. [CrossRef]
23. Meng, F.; Wang, J.; Li, T.; Fang, C. Pollution Characteristics, Transport Pathways, and Potential Source Regions of $PM_{2.5}$ and PM_{10} in Changchun City in 2018. *Int. J. Environ. Res. Public Health* **2020**, *17*, 6585. [CrossRef]
24. Mao, M.; Zhang, X.; Shao, Y.; Yin, Y. Spatiotemporal Variations and Factors of Air Quality in Urban Central China during 2013–2015. *Int. J. Environ. Res. Public Health* **2019**, *17*, 229. [CrossRef] [PubMed]
25. Gong, D.Y.; Guo, D.; Ho, C.H. Weekend effect in diurnal temperature range in China: Opposite signals between winter and summer. *J. Geophys. Res. Earth Surf.* **2006**, *111*, D18113. [CrossRef]
26. An, J.; Shi, Y.; Wang, J.; Zhu, B. Temporal Variations of O3 and NO x in the Urban Background Atmosphere of Nanjing, East China. *Arch. Environ. Contam. Toxicol.* **2016**, *71*, 224–234. [CrossRef] [PubMed]
27. Lebron, F. A comparison of weekend-weekday ozone and hydrocarbon concentrations in the Baltimore-Washington metropolitan area. *Atmos. Environ.* **1975**, *9*, 861–863. [CrossRef]
28. Sadanaga, Y.; Shibata, S.; Hamana, M.; Takenaka, N.; Bandow, H. Weekday/weekend difference of ozone and its precursors in urban areas of Japan, focusing on nitrogen oxides and hydrocarbons. *Atmos. Environ.* **2008**, *42*, 4708–4723. [CrossRef]
29. de Keijzer, C.; Agis, D.; Ambrós, A.; Arévalo, G.; Baldasano, J.M.; Bande, S.; Barrera-Gómez, J.; Benach, J.; Cirach, M.; Dadvand, P.; et al. The association of air pollution and greenness with mortality and life expectancy in Spain: A small-area study. *Environ. Int.* **2017**, *99*, 170–176. [CrossRef] [PubMed]
30. Yu, H.; Feng, J.; Su, X.; Li, Y.; Sun, J. A seriously air pollution area affected by anthropogenic in the central China: Temporal–spatial distribution and potential sources. *Environ. Geochem. Health* **2020**, *42*, 3199–3211. [CrossRef]
31. Wen, X.; Chen, W.; Chen, B.; Yang, C.; Tu, G.; Cheng, T. Does the prohibition on open burning of straw mitigate air pollution? An empirical study in Jilin Province of China in the post-harvest season. *J. Environ. Manag.* **2020**, *264*, 110451. [CrossRef]
32. Fernández-Fernández, M.I.; Gallego, M.C.; Garcia, J.A.; Acero, F.J. A study of surface ozone variability over the Iberian Peninsula during the last fifty years. *Atmos. Environ.* **2011**, *45*, 1946–1959. [CrossRef]
33. Zhang, F.; Wang, Z.; Cheng, H.; Lv, X.; Gong, W.; Wang, X.; Zhang, G. Seasonal variations and chemical characteristics of PM2.5 in Wuhan, central China. *Sci. Total Environ.* **2015**, *518*, 97–105. [CrossRef]
34. Chen, W.; Li, J.; Bao, Q.; Gao, Z.; Cheng, T.; Yu, Y. Evaluation of Straw Open Burning Prohibition Effect on Provincial Air Quality during October and November 2018 in Jilin Province. *Atmosphere* **2019**, *10*, 375. [CrossRef]
35. Liu, J. Study on Temporal and Spatial Variation Law and Evaluation and Prediction Model of Air Pollutants in Beijing. Ph.D. Thesis, Beijing University of Science and Technology, Beijing, China, 2015.
36. Lamsal, L.N.; Martin, R.V.; Van Donkelaar, A.; Celarier, E.A.; Bucsela, E.J.; Boersma, K.F.; Dirksen, R.; Luo, C.; Wang, Y. Indirect validation of tropospheric nitrogen dioxide retrieved from the OMI satellite instrument: Insight into the seasonal variation of nitrogen oxides at northern midlatitudes. *J. Geophys. Res. Earth Surf.* **2010**, *115*, D05302. [CrossRef]
37. Wang, J.; Xie, X.; Fang, C. Temporal and Spatial Distribution Characteristics of Atmospheric Particulate Matter (PM10 and PM2.5) in Changchun and Analysis of Its Influencing Factors. *Atmosphere* **2019**, *10*, 651. [CrossRef]
38. Tang, G.; Zhang, J.; Zhu, X.; Song, T.; Münkel, C.; Hu, B.; Schäfer, K.; Liu, Z.; Zhang, J.; Wang, L.; et al. Mixing layer height and its implications for air pollution over Beijing, China. *Atmos. Chem. Phys.* **2016**, *16*, 2459–2475. [CrossRef]
39. Yao, L.; Lu, N.; Yue, X.; Du, J.; Yang, C. Comparison of Hourly PM2.5 Observations Between Urban and Suburban Areas in Beijing, China. *Int. J. Environ. Res. Public Health* **2015**, *12*, 12264–12276. [CrossRef] [PubMed]
40. Wang, Y.; Duan, X.; Wang, L. Spatial-Temporal Evolution of PM2.5 Concentration and its Socioeconomic Influence Factors in Chinese Cities in 2014–2017. *Int. J. Environ. Res. Public Health* **2019**, *16*, 985. [CrossRef]
41. Boynard, A.; Clerbaux, C.; Clarisse, L.; Safieddine, S.; Pommier, M.; Van Damme, M.; Bauduin, S.; Oudot, C.; Hadji-Lazaro, J.; Hurtmans, D.; et al. First simultaneous space measurements of atmospheric pollutants in the boundary layer from IASI: A case study in the North China Plain. *Geophys. Res. Lett.* **2013**, *41*, 645–651. [CrossRef]
42. Seguel, R.J.; Morales, S.R.G.E.; Leiva, G.M.A. Ozone weekend effect in Santiago, Chile. *Environ. Pollut.* **2012**, *162*, 72–79. [CrossRef]
43. Tang, W.; Zhao, C.; Geng, F.; Peng, L.; Zhou, G.; Gao, W.; Xu, J.; Tie, X. Study of ozone "weekend effect" in Shanghai. *Sci. China Ser. D Earth Sci.* **2008**, *51*, 1354–1360. [CrossRef]
44. Atkinson-Palombo, C.M.; Miller, J.A.; Ballingjr, R.C., Jr. Quantifying the ozone "weekend effect" at various locations in Phoenix, Arizona. *Atmos. Environ.* **2006**, *40*, 7644–7658. [CrossRef]
45. Zou, Y.; Charlesworth, E.; Yin, C.; Yan, X.; Deng, X.; Li, F. The weekday/weekend ozone differences induced by the emissions change during summer and autumn in Guangzhou, China. *Atmos. Environ.* **2019**, *199*, 114–126. [CrossRef]
46. Blanchard, C.L.; Tanenbaum, S.J. Differences between Weekday and Weekend Air Pollutant Levels in Southern California. *J. Air Waste Manag. Assoc.* **2003**, *53*, 816–828. [CrossRef] [PubMed]
47. Wolff, G.T.; Kahlbaum, D.F.; Heuss, J.M. The vanishing ozone weekday/weekend effect. *J. Air Waste Manag. Assoc.* **2013**, *63*, 292–299. [CrossRef] [PubMed]